EUROPEAN ORGANIZATION FOR NUCLEAR RESEARCH

CORRELATIONS OF SECONDARIES IN EVENTS WITH A FORWARD NEGATIVE HADRON AT THE ISR

U. Amaldi, W. Bartel*), G. Cocconi, A.N. Diddens, Z. Dimcovski, R.W. Dobinson, P. Duinker*), A.M. Thorndike**) and A.M. Wetherell

CERN, Geneva, Switzerland

G. Bellettini***), P.L. Braccini, R. Castaldi†, T. Del Prete, P. Laurelli†, G. Sanguinetti and M. Valdata

Istituto Nazionale di Fisica Nucleare, Sezione di Pisa, Italy
Istituto di Fisica dell'Università, Pisa, Italy

A. Baroncelli and G. Matthiae†

Physics Laboratory, Istituto Superiore di Sanità
and INFN, Sezione Sanità, Rome, Italy

P. Grannis, H. Jöstlein, R. Kephart, D. Lloyd-Owen, and R. Thun

State University of New York, Stony Brook, New York, USA

ABSTRACT

Data, obtained from p-p collisions at centre-of-mass energies between 31 and 63 GeV, are presented on correlations between momentum analysed forward π^-, K^- and $\bar{p}$ and charged particles observed in an omnidirectional hodoscope. The data show that significant correlations are present over the whole rapidity range for all three types of negative particles. The dependence on various kinematic variables suggests a cluster mechanism for the production of particles. In this picture, pions would be produced in clusters emitted in the fragmentation region while K^- and $\bar{p}$ emanate from non-leading clusters.

Submitted to Physics Letters

9 June 1975

---

*) Present address: DESY, Hamburg, Germany

**) On leave from Brookhaven National Laboratory, Upton, New York, USA.

***) Present address: Laboratori Nazionali del CNEN, and INFN, Sezione di Frascati, Frascati, Italy.

†) Also at CERN, Geneva, Switzerland.

Results from a study of the correlations between charged particles and momentum-analysed π^-, K^- and $\bar{p}$ produced in pp collisions at the CERN Intersecting Storage Rings (ISR) are presented.

The apparatus consisted of a small aperture magnetic spectrometer[1] (CERN-Rome group) and a counter hodoscope system[2] (Pisa-Stony Brook group) covering nearly the complete solid angle. The angular correlations between the negatively charged particles detected in the spectrometer and the over-all distribution of charged secondaries observed in the hodoscope were studied for centre-of-mass energies $\sqrt{s}$ of 31, 45, 53 and 63 GeV.

The magnetic spectrometer detected negatively charged particles emitted at essentially 0° with respect to one of the two colliding beams. The solid angle was $\Delta\Omega \simeq 4$ μsr, the momentum acceptance was $\Delta p/p \simeq \pm 12\%$ and the momentum resolution about 1%. Particles were identified by four threshold Cerenkov counters and their trajectories determined by means of twelve planes of multiwire proportional chambers. The range of secondary particle momenta detected in the spectrometer corresponded to $0.4 < x < 1$, where

$$x = p/p_0$$

is the ratio of the secondary particle momentum p to the primary momentum p_0.

The hodoscope system consisted of large arrays of detectors (about 350 scintillation counters) covering about 80% of the full solid angle around the colliding beams region. Inelastic collisions were detected with an efficiency of about 97%. The counters were subdivided in such a way as to measure the polar angle of charged secondaries in 43 independent bins. The minimum angle which could be detected was about 10 mrad. Since the hodoscope system measured only emission angles and not particle momenta, the data are presented in terms of the variable.

$$\eta = -\ln\left(\operatorname{tg}\frac{\theta}{2}\right) \qquad (1)$$

where θ is defined as the polar angle with respect to the proton beams. Positive η corresponds to particles emitted in the hemisphere containing the spectrometer and negative η to particles emitted in the opposite hemisphere. The maximum value of η attainable was 5.3. For the angular range accepted by the hodoscope the variable η is to a good approximation equal to the rapidity

$$y = \sinh^{-1}\frac{P_L}{\sqrt{m^2 + P_T^2}}, \qquad (2)$$

as $(m/P_T)^2 << 1$. In Eq. (2) m is the mass, and P_L and P_T are, respectively, the longitudinal and transverse momentum components of the particle.

The rapidity y of the spectrometer particle is determined by its angle and momentum. Its relation with the variable x is given by

$$y_{max} - y \approx -\ln x \tag{3}$$

for $p >> m$, where $y_{max} = \ln(\sqrt{s}/m)$ is the maximum allowed rapidity of a particle of a given mass. For $x \geq 0.4$, it follows that $y_{max} - y \leq 0.9$, and therefore the spectrometer particle always belongs to the so-called fragmentation region.

Correlations between the spectrometer particle and any particle detected by the hodoscope will be expressed in terms of the standard two-body correlation function

$$R(\eta,y) = \frac{\sigma_{in} d^2\sigma/d\eta dy}{d\sigma/d\eta \cdot d\sigma/dy} - 1, \tag{4}$$

where σ_{in} is the total inelastic cross-section; y is used for the spectrometer and η for the hodoscope. For a fixed y in the spectrometer, $R(\eta)$ can be written in terms of the observed counting rates as

$$R(\eta) = \frac{\Delta N_c(\eta) \ / \ T_c}{\Delta N_0(\eta) \ / \ T_0} - 1 \ , \tag{5}$$

where the subscripts denote the two different trigger conditions: trigger (c) required a coincidence between one particle in the spectrometer and at least one charged particle in each hemisphere of the hodoscope; the only requirement for the unbiased trigger (o) was the presence of at least one charged particle in each hemisphere of the hodoscope system. In Eq. (5) T_c and T_0 are the total number of inelastic triggers of the two types indicated, and $\Delta N_c(\eta)$ and $\Delta N_0(\eta)$ are the number of counts registered by the hodoscope elements in the appropriate η bin. $R(\eta) = 0$ would correspond to no correlation, a situation in which the hodoscope distribution is unaffected by the requirement of a particle detected in the spectrometer. It should be remarked that the correlation function R is free, to a first approximation, from the corrections (due to finite bin size and secondary interactions) needed to deduce true particle multiplicities from those observed in the hodoscope, as only ratios of counting rates are involved.

The x-dependence of the shape of the correlation function for π^- was investigated systematically at centre-of-mass energy $\sqrt{s}$ = 53 GeV. The results are shown in Fig. 1a. For values of η in the central region, i.e. $|\eta| \lesssim 2$, the correlation function is smooth but not flat; it exhibits a slope which increases with x. This behaviour may be expected intuitively, as in the emission of a particle of, say, x = 0.8 there is found to be a depletion of multiplicity in the same hemisphere with respect to that in the opposite. A phase-space calculation by the Monte Carlo method was made in order to estimate the effects of energy-momentum conservation on the correlation function. Events were generated with a realistic multiplicity distribution, a transverse momentum cut-off and leading particle behaviour. The calculation gives results, shown in Fig. 1a, with a trend similar to the observed effect which may, therefore, be partly of kinematic origin.

Fig. 1a shows that at large negative η, $R(\eta)$ exhibits an "enhancement", while for positive η, a bump is found on top of a steadily decreasing continuum; both the bump and the enhancement are much more pronounced at low x. The bump is centred at $\eta \approx 3.7$ and has a full width at half height of about 1.5 units of η. The energy dependence of the bump position was studied for π^- of fixed x = 0.5, where this structure is very prominent. As $\sqrt{s}$ changes from 31 to 45 and 63 GeV, the bump moves from $\eta \simeq 3.4$ to $\eta \simeq 3.7$ and $\eta \simeq 4.1$, following very closely the shift of the π^- rapidity which varies from 4.7 to 5.1 and to 5.4.

The x-dependence of $R(\eta)$ for K^- at $\sqrt{s}$ = 53 GeV was also studied and the results are shown in Fig. 1b. The statistics for kaons is poorer than for pions. It may be concluded, however, that for low values of x, the correlation functions of π^- and K^- have qualitatively similar shapes, while for high values of x, the bump at positive η which is disappearing for π^-, is, on the contrary, still present and perhaps even more prominent for K^-. In addition the enhancement at negative values of η is bigger for large x.

After these general and introductory remarks a more detailed discussion of the results follows. A considerable amount of data was taken at $\sqrt{s}$ = 53 GeV and fixed x = 0.4 to compare the behaviour of the correlations observed for π^-, K^- and $\bar{p}$. On the top line of Fig. 2, the inclusive correlation function $R(\eta)$, as defined by Eqs. (4) and (5), is shown for the three different particles, together with the unbiased η-distribution.

$$\frac{1}{T_0}\frac{\Delta N_0}{\Delta \eta} \, .$$

At x = 0.4 the inclusive correlation functions of $\bar{p}$ are clearly similar to those of π^- and K^-.

In order to elucidate the meaning of the structures observed in $R(\eta)$, a study of the semi-inclusive correlation function was made by selecting events having a given total multiplicity of charged secondaries. The semi-inclusive correlation function $R_n(\eta)$ is defined as previously in Eqs. (4) and (5), where now the index n refers to the subset of events having a total observed multiplicity equal to n. With this definition the multiplicity measured by the hodoscope with trigger conditions (o) and (c) is n and (n-1) respectively. It has to be noted that the multiplicity distribution observed by the hodoscope contains odd as well as even values of n, this is a consequence of losses and secondary interactions.

The evaluation of the semi-inclusive correlation functions was done by grouping the events in the following intervals of multiplicity: n = 4-5, n = 6-9, n = 10-17 and $n \geq 18$. In Fig. 2a the unbiased η-distributions of the secondaries, as measured by the hodoscope with trigger (o) at $\sqrt{s}$ = 53 GeV are shown for these four classes of multiplicity, together with the correlation functions for π^-, K^- and $\bar{p}$ at x = 0.4 in Figs. 2b, 2c, and 2d, respectively.

The π^- data, shown in Fig. 2b will be discussed first. It is clear that both the enhancement and the bump which are seen in the $R(\eta)$ function at the two extremes of the η range, are mainly low-multiplicity phenomena. The simplest interpretation is that these structures are produced by the events where the proton, incident toward the spectrometer, fragments into a rather small number of particles. The bump at positive η therefore indicates the presence of a cluster of particles accompanying the π^-. The enhancement at negative η, which appears to follow in size the bump, is, for the events with single fragmentation, a reflection of the presence of the bump itself as imposed by the need for balancing the momentum. Additional contributions to this enhancement may come from double fragmentation. The interpretation of the bump, as a particle clustering effect in the fragmentation region, is also substantiated by the observation of the shift with energy mentioned earlier.

The prominence of the bump for π^- at low x is easily understood as a kinematical effect; a cluster, resulting from the fragmentation of one of the incident protons, will in fact always contain a nucleon which carries most of the cluster momentum, while the pion, on the average, remains with lower momentum. The same kinematical argument could explain why for kaons, which have a larger mass, $R(\eta)$ still shows a bump at positive η for high values of x. The average mass of the π cluster was estimated by beams of a Monte Carlo calculation from the corresponding value of η and was found to be about 2 GeV.

In order to understand the character of the cluster, a study was made of the events with total observed multiplicity n = 4 which include the process

$$pp \rightarrow pp\pi^+\pi^- \quad . \tag{6}$$

A large fraction of these events had a hocoscope configuration with one particle emitted at very small angles in the hemisphere opposite to the spectrometer and two particles at rather small angles relative to the π^- detected in the spectrometer. A consistency requirement imposed by the balancing of transverse momentum reduced the sample to about 25%, the rejected events most likely containing one or more neutral pions. For the remaining events the cluster consisted then presumably of a $(p\pi^+\pi^-)$ system. The effective mass of this system was calculated by assuming that, of the two particles detected by the hodoscope on the spectrometer side, the one emitted with smaller polar angle θ, was the proton. Under this assumption, which a Monte Carlo calculation has shown to be true for at least 90% of the events, the $(p\pi^+\pi^-)$ mass was calculated and found to peak around 2 GeV. The momentum transfer distribution of these events had a forward peak with an average slope of ~ 10 GeV^{-2}. The observed slope was found to be a function of the mass of the $(p\pi\pi)$ system and decreased from 14 GeV^{-2} to 8 GeV^{-2} when the mass increased from 1.5 up to 4 GeV. The integrated production cross section corresponding to reaction (6) is then 0.4 ± 0.2 mb, where a factor of two has been included to account for the forward-backward symmetry. Momentum transfer distributions and the cross-section of the multiplicity n = 4 events are similar to those previously reported[3] for process (6) at FNAL and at the ISR.

An attempt was also made to extract the average charged particle multiplicity of the cluster by applying the same method[4] which has been used to obtain the central cluster multiplicity from correlation data in the central region. This consists, essentially, of determining the height of the bump above the smooth background and was done by making a linear extrapolation of the smooth continuum below the structure in the function $R(\eta)$. It was thus found that the average charged multiplicity of the cluster containing a π^- was about 4; the same value was obtained for clusters containing a K^- or a $\bar{p}$.

It may be concluded that for pions produced in low multiplicity events the bump in the function $R(\eta)$ reflects the production of a cluster in the fragmentation region of one of the colliding protons, i.e. of a "leading cluster" with baryon number +1. In the limiting case of very small multiplicity, when the cluster corresponds to the $(p\pi\pi)$ system, the production mechanism may be identified with a diffractive-like process. Further support for this is given by the

distribution of associated particle multiplicities (Fig. 3), which shows that when a π^- is detected in the spectrometer the relative probability for observing events with n = 4-5 is considerably greater than in the unbiased case. Observations[5] of neutron correlations, in an associated experiment, lead to similar conclusions, in fact, it appears that detection of a neutron or of a π^- in the fragmentation region represent complementary ways for demonstrating the production of leading clusters.

The data on K^- and $\bar{p}$ production will now be discussed. These events are, of course, quite rare, the K^-/π^- and $\bar{p}/\pi^-$ ratios being only about 6% and 1.5%, respectively, at x = 0.4 and 0^o. The similarity of the inclusive correlation functions for $\bar{p}$ and K^- to that for π^- at x = 0.4, exhibited in Fig. 2, suggests, without further consideration, the possibility that the production mechanisms of K^- and $\bar{p}$ are similar to that of π^-. An analysis for K^- and $\bar{p}$ events with n = 4, assuming that the clusters correspond to (pK^+K^-) and $(pp\bar{p})$ systems, gives cluster masses of 2.5 GeV and 4 GeV, respectively. The differences between the data for K^-, $\bar{p}$ and π^-, shown in Figs. 1, 2, and 3, are, however, considerable and suggest that the mechanisms involved are different. The differences may be listed as follows:

i) Fig. 1 shows that the cluster structure for K^- persists and becomes perhaps even more prominent with increasing x up to x = 0.8 while that for π^- does not.

ii) Fig. 2 indicates that, at fixed x (= 0.4), the structure for K^- and $\bar{p}$ remains prominent for the highest multiplicities while that for π^- decreases with increase of n.

iii) Fig. 3 shows a great enhancement (narrow peak) of multiplicity at low n for π^-, while for K^- and $\bar{p}$ there is an enrichment at large n (10-16).

iv) Fig. 2 shows that although the K^- and $\bar{p}$ exhibit a bump at $\eta \simeq 4$, for multiplicities 4-5, similar to that observed for the π^-, at $\eta \simeq 0$ $R(\eta)$ is almost zero for K^- and $\bar{p}$ while $R(\eta) \simeq -0.8$ for π^-, indicating a factor of ~ 5 more in relative particle density in the central region for K^- and $\bar{p}$.

In addition, the inclusive distributions[1] $E\, d^2\sigma/d\vec{p}^3$ for K^- and $\bar{p}$ decrease much more strongly with increasing x than in the case for π^-, a feature also observed at lower energies[6].

The masses of the clusters which are parents to the K^- and $\bar{p}$ are not very high, as the decay particles detected in the hodoscope system appear at small angles relative to the K^- or $\bar{p}$ in the spectrometer. Thus, although the formation of light clusters appears to be a common feature of π^-, K^- and $\bar{p}$ production in the fragmentation region, the facts (i) to (iv) outlined above suggest that the cluster production mechanism for K^- and $\bar{p}$ is different from that for π^-. The frequent production of leading clusters containing K^- or $\bar{p}$ is also rendered implausible by the observation[7] that the mean multiplicity in the decay of leading clusters, of mass M_c, is essentially the same as the multiplicity found in hadron collisions of total energy $\sqrt{s}$, such that $\sqrt{s} = M_c$. For this condition it is plausible that the relative abundances of the particles emitted in the cluster decay should be similar to that in a hadronic production process at the corresponding energy. This expectation would lead to a relative $\bar{p}$ abundance of the order of 10^{-4}, much lower than the 1.5% noted above.

The most appropriate mechanism to invoke in the present circumstances, particularly in view of points (ii), (iii) and (iv) which show that high multiplicities are indeed characteristic of $\bar{p}$ production is, then, that highly inelastic collisions produce non-leading clusters which decay into the heavy particles together with a general particle "boil off" in the central region. These non-leading clusters may have either zero baryon number (mesonic clusters) or negative baryon number (anti-clusters). The present experiment cannot decide between the two possibilities as the other particles associated with the $\bar{p}$ are not identified.

As the K^- correlation patterns are very similar to those for $\bar{p}$ it is plausible that the K^- also result from non-leading cluster decay. Clusters of positive, negative and of zero baryon number could very well contribute to the K^- production observed. With regard to the last possibility, namely a parent mesonic cluster, it is interesting to note in Fig. 2c, for n = 4-5, a narrow enhancement in the K^- correlation function at $\eta \simeq 4.3$. This enhancement is consistent, kinematically, with the decay of ϕ mesons produced at $x \simeq 0.8$ into a $K\bar{K}$ pair, each particle with $x = 0.4$ and the opening angle between them being small because of the low kinetic energy available in the decay. If this were so, about 5% of the K^- observed at $x = 0.4$ could be attributed to ϕ mesons produced in the forward direction at $x = 0.8$.

To summarize, the following main conclusions are suggested by the data:

a) π^- produced at 0^o in the fragmentation region in low multiplicity events are the decay products of leading clusters of positive baryon number formed by a diffractive mechanism; cluster production with emission of forward π^- in high multiplicity events is relatively less abundant.

b) $\bar{p}$ observed in the fragmentation region are often produced in highly inelastic collisions, in which non-leading clusters, either mesonic or anti-baryonic, are formed, the $\bar{p}$ being among the products of the disintegration of such clusters.

c) K^- also often originate from non-leading clusters formed in highly inelastic collisions.

We are indebted to the personnel of the ISR Department for their many contributions to this experiment. In particular we are grateful to G. Kantardjian for his co-ordination of technical services and to M. Wensveen for installations. J-C. Brunet, J-C. Godot and E. Jones are to be thanked for their work on a special vacuum chamber and M. Harris for the design and construction of the movable spectrometer. We are grateful to M. Busi for much effort in the data reduction and to J.V. Allaby, C. Bosio, J. Dorenbosch and W. Duinker for help in various phases of the experiment. We thank A. Bechini, R. Donnet and M. Ferrat for their excellent technical support.

REFERENCES

1) U. Amaldi et al., (to be published).
Thesis of Z. Dimcovski, NP Internal Report 74-8, 17 October 1974.

2) S.R. Amendolia et al., Nuovo Cimento 17A, 735 (1973).
S.R. Amendolia et al., Proc. 1973 Int. Conf. on Instrumentation for High Energy Physics (Frascati), p.391.

3) M. Derrick et al., Phys. Rev. D9, 1215 (1975).
L. Baksay et al., Physics Letters 53B, 484 (1975).

4) E.L. Berger and G.C. Fox, Phys. Letters 47B, 162 (1973).
W. Schmidt-Parzefall, Phys. Letters 46B, 399 (1973).

5) U. Amaldi et al., following letter.

6) U. Amaldi et al., Nuc. Physics 38b, 403 (1975).

7) S.J. Barish et al., Phys. Rev. Letters 31, 1080 (1973).

FIGURE CAPTIONS

Fig. 1 : The correlation function $R(\eta)$ at $\sqrt{s}$ = 53 GeV for π^- and K^- detected in the spectrometer with fractional momentum x, is plotted as a function of the variable η.
a) $R(\eta)$ for π^- of x = 0.4, 0.6, and 0.8.
b) $R(\eta)$ for K^- of x = 0.4, 0.6, and 0.8.
The broken lines in Fig. 1a are the result of the phase-space calculation discussed in the text.

Fig. 2 : The unbiased η-distributions of the charged secondaries as measured by the hodoscope with trigger (o) at $\sqrt{s}$ = 53 GeV are shown in Fig. 2a. These distributions have been smoothed and should be regarded as qualitative. The correlation functions, at $\sqrt{s}$ = 53 GeV, for π^-, K^- and $\bar{p}$ of x = 0.4 are shown in Fig. 2b, 2c and 2d, respectively. The top line contains the inclusive, unbiased, η-distribution and the inclusive $R(\eta)$ functions. The other lines contain the semi-inclusive, unbiased, η-distributions and the corresponding semi-inclusive $R_n(\eta)$ functions for the multiplicity intervals : n = 4-5, n ≃ 6-9, n = 10-17 and n ≳ 18.

Fig. 3 : Multiplicity distributions of charged secondaries at $\sqrt{s}$ = 53 GeV for the events with a π^-, K^- or $\bar{p}$ of x = 0.4 emitted in the forward direction. The distributions are raw data and have not been corrected for secondary interactions of the produced particles. The fraction of events with total multiplicity equal to n is shown as a function of n for the three different particles. The solid line represents the multiplicity distribution observed with trigger (o), i.e. without requiring the coincidence with the spectrometer particle.

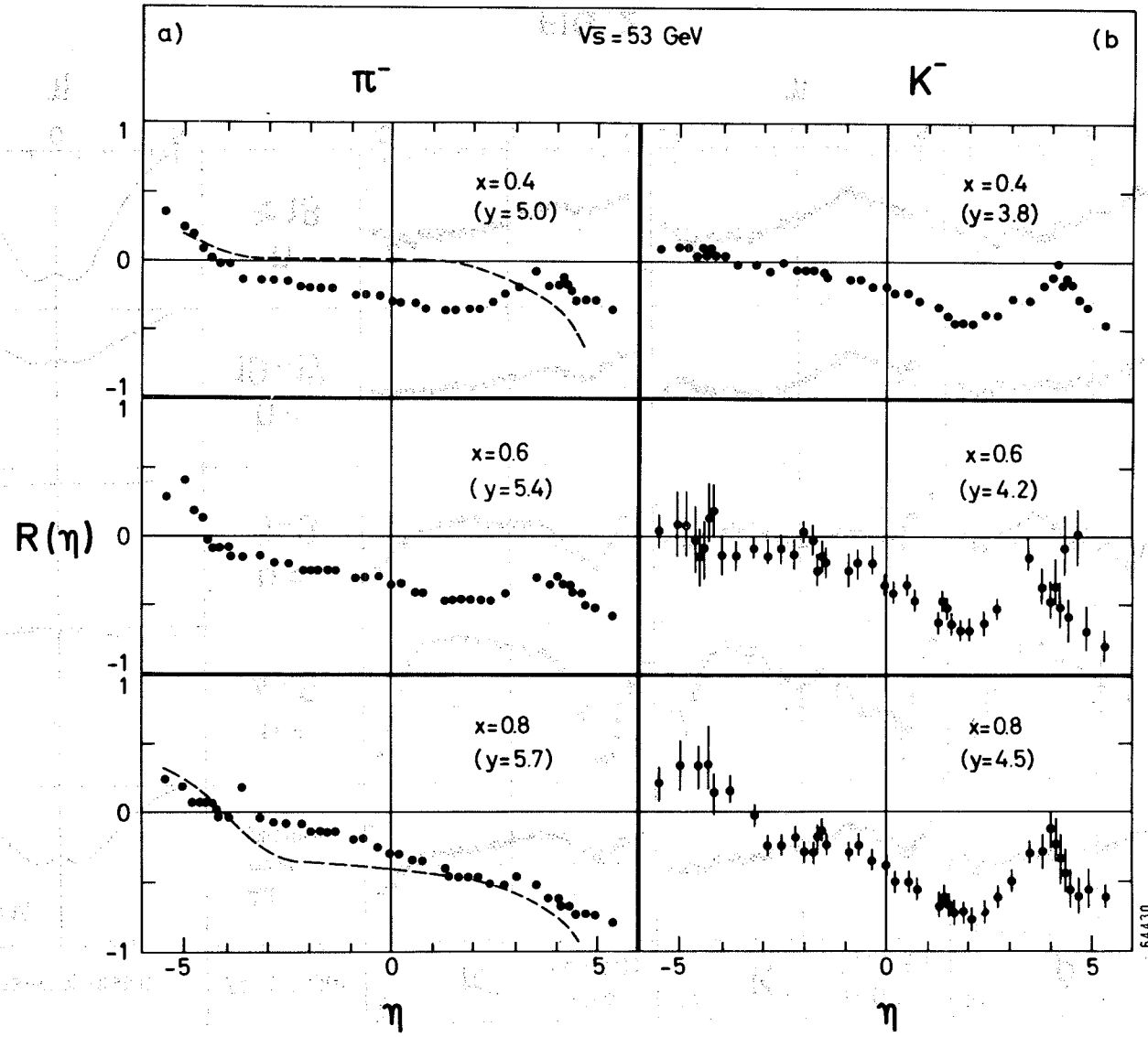
a)
√s = 53 GeV
(b
π⁻
K⁻
x=0.4
(y=5.0)
x=0.4
(y=3.8)
x=0.6
(y=5.4)
x=0.6
(y=4.2)
x=0.8
(y=5.7)
x=0.8
(y=4.5)
R(η)
η
η
64430

FIG:1

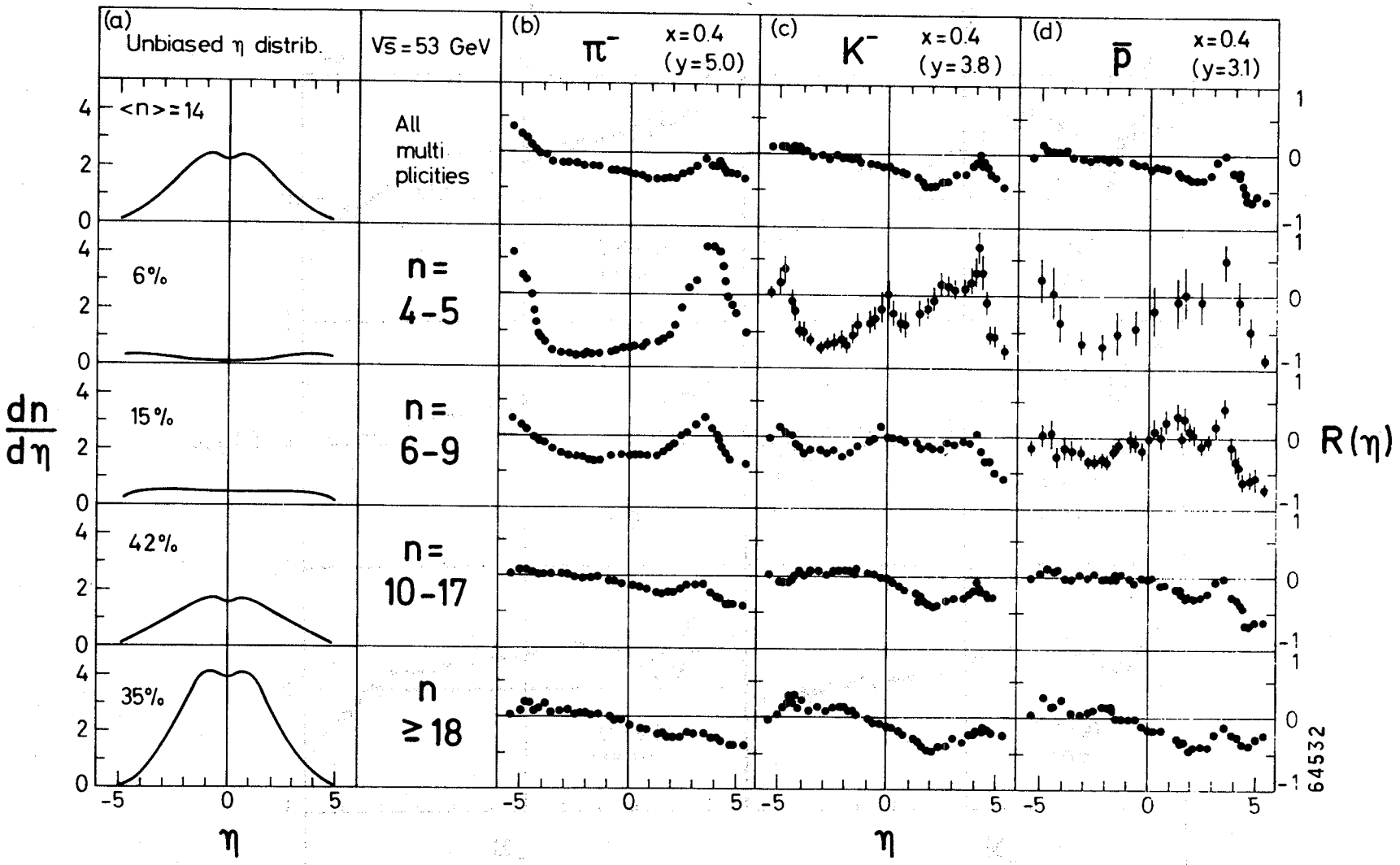
(a)
Unbiased η distrib.
√s = 53 GeV
(b) π⁻ x = 0.4 (y = 5.0)
(c) K⁻ x = 0.4 (y = 3.8)
(d) p̄ x = 0.4 (y = 3.1)
<n> = 14
All multiplicities
6%
n = 4-5
15%
n = 6-9
42%
n = 10-17
35%
n ≥ 18
dn/dη
R(η)
η
η
64532

FIG:2

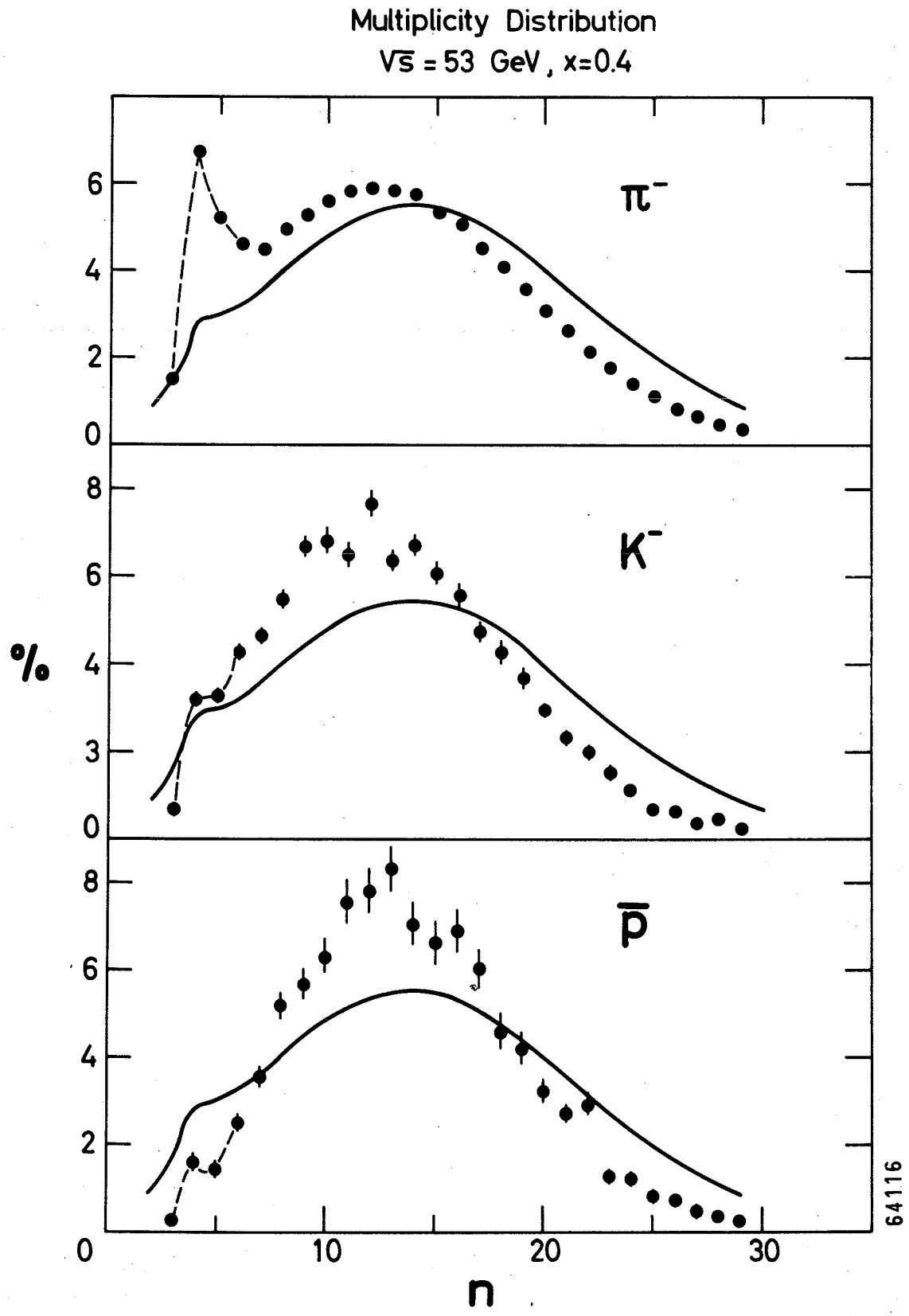
Multiplicity Distribution
√s = 53 GeV, x=0.4
π⁻
K⁻
p̄
%
n
0
2
4
6
8
10
20
30
64116

FIG:3